HuD (ELAVL4) gain-of-function impairs neuromuscular junctions and induces apoptosis in familial and sporadic amyotrophic lateral sclerosis models

Beatrice Silvestri[1,2], Michela Mochi[1], Darilang Mawrie[3], Valeria de Turris[2], Alessio Colantoni[1,2], Beatrice Borhy[1], Maria Giovanna Garone[4], Christopher Patrick Zammerilla[3], Udai B. Pandey[3] and Alessandro Rosa[1,2,*]

1. Department of Biology and Biotechnologies “Charles Darwin”, Sapienza University of Rome, Rome, Italy.
2. Center for Life Nano- & Neuro-Science, Fondazione Istituto Italiano di Tecnologia (IIT), Rome, Italy.
3. Department of Pediatrics and Neurology, University of Pittsburgh Medical Center, PA, USA.
4. Department of Stem Cell Biology, Murdoch Children’s Research Institute, The Royal Children's Hospital, Parkville, Melbourne, Victoria, Australia.

* corresponding author: alessandro.rosa@uniroma1.it

KEYWORDS: HuD; ELAVL4; FUS; amyotrophic lateral sclerosis; neuromuscular junction; iPS cells; Drosophila; elav; GAP43; NRN1

ABSTRACT

Early defects at the neuromuscular junction (NMJ) are among the first hallmarks of the progressive neurodegenerative disease amyotrophic lateral sclerosis (ALS). According to the "dying back" hypothesis, disruption of the NMJ not only precedes, but is also a trigger for the subsequent degeneration of the motoneuron. However, the pathogenic mechanisms linking genetic and environmental factors to NMJ defects remain elusive. Here we show that increased expression of the neural RNA binding protein HuD (ELAVL4) at the presynaptic level is sufficient to cause NMJ defects and trigger apoptosis in co-cultures of motoneurons and skeletal muscle derived from human induced pluripotent stem cells (iPSCs). These phenotypes are strikingly similar to those caused by the severe FUS P525L variant. Moreover, HuD knock-down in motoneurons reverts the adverse effects of the FUS^{P525L} mutation in iPSC-derived co-cultures. These findings were validated *in vivo* by taking advantage of a *Drosophila* model, where neuronal-restricted overexpression of the HuD-related gene, *elav*, exacerbates the effects of FUS expression and produces *per se* a motor phenotype. Notably, in this fly model, neuronal-restricted *elav* knockdown significantly rescues motor dysfunction caused by FUS. Finally, we show that HuD levels are increased upon oxidative stress in human motoneurons, and in sporadic ALS patients with a signature related to oxidative stress. On these bases, we propose HuD as a key protein involved in causing early pathogenic alterations and offers a potential new therapeutic target for early intervention aimed at the NMJ in ALS.

INTRODUCTION

The neurodegenerative disease amyotrophic lateral sclerosis (ALS) is caused by progressive loss of skeletal muscle function due to motoneuron (MN) death (Brown & Al-Chalabi, 2017). While the vast majority of cases are considered sporadic, genetic variants in individual, ubiquitously expressed, RNA-binding proteins (RBPs) have been linked to ALS. In the nervous system, ubiquitous and neural-specific RBPs cooperate in gene expression regulation and cross-regulation and feedback loops are crucial in establishing proper levels and activity of each RBP (Dassi, 2017). An extensive crosstalk also exists between ubiquitous ALS-linked RBPs, such as FUS, and other neural RBPs expressed in the MN (Blokhuis et al., 2016; De Santis et al., 2019). Thus, in the MN, ALS-associated genetic variants in one node of the network might impact other RBPs and produce broader, unexpected, effects that could be highly cell-type specific. In this context, we have previously shown that mRNA and protein levels of HuD, encoded by the *ELAVL4* gene, are upregulated in MNs derived from *FUS* mutant human induced pluripotent stem cells (iPSCs) and in a mouse model (Fus-Δ14 knock-in) (Garone et al., 2021). This could be due to the combined effects of downregulation of miR-375, a HuD targeting miRNA (De Santis et al., 2017), and direct binding of mutant FUS to *HuD* 3'UTR, resulting in competition between mutant FUS and FMRP for *HuD* 3'UTR binding (De Santis et al., 2019; Garone et al., 2021). Increased HuD levels in FUS^{WT} MNs produce changes in the transcriptome that are substantially similar to those exerted by the severe *FUS* P525L variant (Garone et al., 2023). A direct consequence of HuD upregulation in FUS mutant iPSC-derived MNs and mouse spinal cord is an increase of the levels of two previously known HuD targets, Neuritin1 (NRN1; also known as cpg15) and GAP43 (Garone et al., 2021). By stabilizing and localizing these and other target mRNAs through 3'UTR binding, HuD plays key roles during nervous system development (Bronicki and Jasmin, 2013). However, recent evidence points to its possible involvement in neurodegenerative processes as well (Silvestri et al., 2022). Increased HuD protein levels have also been recently found in post-mortem sporadic ALS patients' motor cortex (Dell'Orco et al., 2021).

In this work we aimed to assess if HuD dysregulation could underlie neuromuscular junctions (NMJs) defects in the context of ALS. Several genes that are commonly altered in FUS^{P525L} MNs and HuD overexpressing MNs are involved in axon projection, cell junction and synapse formation (Garone et al., 2020; Garone et al., 2023). ALS is considered a distal axonopathy as early impairment of NMJs has been reported in both animal models and patients. These include $SOD1^{G93A}$ mice, in which endplate denervation, followed by ventral root axons degeneration, occurs way before the death of MNs in the spinal cord (Fischer et al., 2004). Notably, such ''dying back'' pattern was also evident in a sporadic ALS patient who unexpectedly died few weeks after the diagnosis (Fischer et al., 2004), and recently proposed for familial ALS linked to RBP genes, including *FUS*. To this regard, knock-in mouse models have provided important information. Lower MNs loss due to increased apoptosis was observed at birth in a mouse model carrying a homozygous truncation in the C-terminal domain abolishing the nuclear localization signal ($Fus^{\Delta NLS/\Delta NLS}$; Scekic-Zahirovic et al., 2016). Notably, this was due to toxic gain of function of the mutant protein, rather than loss of nuclear functions, as the MN number was not reduced in $Fus^{-/-}$ mice. Moreover, MN loss in $Fus^{\Delta NLS/\Delta NLS}$ mice occurred in the absence of FUS protein aggregation and stress granules formation and was rescued by MN-specific

reversion of FUS mislocalization (Scekic-Zahirovic et al., 2016). These findings point to cell-autonomous mechanisms leading to MN death which are due to the gain of toxic cytoplasmatic functions of the FUS mutant protein and are independent from its aggregation. A direct causal link between *FUS* variants and NMJ defects was demonstrated by Picchiarelli et al., who showed a reduction in the number and area of the endplates in newborn *Fus*$^{\Delta NLS/\Delta NLS}$ mice (Picchiarelli et al., 2019). Selective restoration of FUS nuclear localization in the muscle rescued the size of the endplate, showing that in mouse this phenotype was due to cell-autonomous toxicity of mutant FUS in skeletal muscle. Progressive denervation and reduction of the endplate size were observed in adult heterozygous mutants (*Fus*$^{\Delta NLS/+}$). Mechanistically, the authors proposed that innervation induces FUS enrichment in subsynaptic muscle nuclei, where it promotes expression of *Chrn* genes at the transcriptional level by synergizing with the transcription factor ERM. Consistently, in human iPSC-derived muscle cells, FUS promotes transcription of the AChR alpha 1 subunit. Moreover, co-cultures of human iPSC-derived wild-type MNs with ALS-FUS mutant skeletal muscle cells (SkMCs) showed defective endplate maturation (Picchiarelli et al., 2019). However, defective transcription of AChR subunits in the muscle due to intrinsic FUS toxicity cannot be considered the sole underlying mechanism for the observed NMJ defects, as *FUS* mutation in MNs exerted a similar maturation phenotype upon co-culture with wild-type SkMCs in the absence of any difference in AChR genes expression in the muscle (Picchiarelli et al., 2019). Decreased number of NMJs per myotube and impaired NMJ maturation were also observed in co-cultures of mutant FUS iPSC-derived MNs and human myotubes derived from mesoangioblasts (MAB) from a healthy individual (Stoklund Dittlau et al., 2021).
Here we found that HuD gain-of-function can account for most of the cell-autonomous effects of a severe *FUS* variant in the MN. These include defective maturation of the NMJ and apoptosis, possibly by a “dying back” pattern, in co-cultures of iPSC-derived MNs and SkMCs. These findings were further supported *in vivo* using a Drosophila model, in which reduction of the *HuD*-related gene *elav* is sufficient to completely rescue the motor phenotype caused by FUS overexpression. We propose that HuD-dependent pathological mechanism directly contribute to sporadic and familial ALS cases.

RESULTS

Establishment of iPSC-derived neuromuscular co-cultures

We have previously developed methods to obtain iPSC derived functional MNs and SkMCs (Lenzi et al., 2016; Garone et al., 2019). In our previous work, however, the protocol to convert iPSCs into SkMCs, which is based on the ectopic expression of MyoD and BAF60c, was used only for short-term cultures (up to 9 days) (Lenzi et al., 2016; Caputo et al., 2020). We noticed that a subpopulation of differentiation resistant cells persisted in longer cultures (Supplementary Fig. S1A-D). Over time, these mitotically active cells outnumbered terminally differentiated SkMCs, thus hindering the establishment of long-term co-cultures. To overcome this problem, we included a step consisting of the transient addition of cytosine arabinoside (AraC), which successfully reduced the number of proliferating undifferentiated cells (Supplementary Fig. S1A-D).

Spinal MN progenitors, generated in 5 days as previously described (Garone et al., 2019), were re-plated onto SkMCs obtained in 13 days with the optimized protocol (Figure 1A,B). Recombinant agrin and laminin proteins were added to the culture medium to promote the expression of post-synaptic AChR subunit genes in muscle cells through the activation of the agrin–LRP4–MuSK–ERM axis, and pre-synaptic differentiation and neurotransmitter release, respectively (Ichikawa et al., 2005; Stoklund Dittlau et al., 2021). After this step, hereafter considered day 0 of the co-culture, we have been able to maintain MNs and SkMCs for further 50 days. Clustering of acetylcholine receptors (AChRs), suggesting the establishment of motor endplate of the neuromuscular junction (NMJ), was detected as early as day 14 (Figure 1C). At day 50, SkMCs show few spontaneous contractions, which were significantly increased by addition of glutamate, to stimulate MNs, and subsequently reduced to zero by addition of curare, a non-depolarizing competitive antagonist of the nicotinic AChR at the NMJ (Figure 1D). Notably, SkMCs cultured in the same conditions, but in absence of MNs, never showed contractions.
Collectively, our data suggests a successful development of a functional neuromuscular model system for mechanistic studies.

NMJ defects due to FUS mutation or HuD overexpression in MNs

Impaired NMJ formation upon FUS mutation in SkMCs, MNs or both had been previously reported (Picchiarelli et al., 2019). We aimed to assess whether the detrimental effect of mutant FUS expression in the MN could be due, at least in part, to increased HuD levels. To this aim, we established co-cultures using MNs from isogenic iPSCs with 3 different genetic backgrounds: FUS^{WT} and FUS^{P525L} (Lenzi et al., 2015), and FUS^{WT} overexpressing HuD under the Synapsin1 promoter (Syn1::HuD; hereafter indicated as "FUS^{WT}+HuD"; Garone et al., 2021) (Figure 2A). Notably, the Synapsin1 promoter confers overexpression of HuD in the range observed in FUS^{P525L} MNs (Garone et al., 2021). In all subsequent experiments, SkMCs have always been derived from FUS^{WT} iPSCs.
After 14 and 28 days, we observed reduction in muscle fibers showing AChR clusters, detected by α-bungarotoxin (αBTX) staining, in the co-cultures established with FUS^{P525L} MNs or upon HuD overexpression (Figure 2B,C). According to our previous observations (Garone et al., 2021), both FUS mutant and HuD overexpressing MNs showed increased neurite network (Figure 2B,C). Thus, the reduction of skeletal muscle cells forming endplates cannot be explained by a reduction in the neuronal component in FUS mutant, or HuD overexpressing, MN co-cultures.
Detailed analysis of the endplate morphology suggested defective maturation when mutant FUS was expressed in the MN, confirming previous observations (Picchiarelli et al., 2019). In particular, we observed a reduced fraction of aligned AChR puncta and endplates categorized as "dense" or "clustered" (Figure 3A,B). Conversely, endplates with diffuse AChR puncta, indicative of an immature formation stage, were significantly increased. Notably, also in this case, HuD upregulation in an otherwise FUS WT genetic background perfectly phenocopied the defects in NMJ maturation produced by the FUS P525L variant.

FUS mutation or HuD overexpression in MNs induced cell death by apoptosis upon co-culture with SkMCs

At late time points, beyond day 28, extensive death of both neuronal and muscle cells was observed in co-cultures containing FUS^{WT} SkMCs in presence of FUS^{P525L} or FUS^{WT}+HuD MNs (Fig. 4A). Quantification of dead cells by staining with fluorescent ethidium homodimer-1 in a time course analysis revealed, for both genotypes, significant difference compared to the FUS^{WT} control (Fig. 4B; Supplementary Figure S2). Notably, we did not find any significant difference between co-cultures made by FUS^{P525L} and FUS^{WT}+HuD MNs. Increased Cleaved Caspase-3 (CC-3) signal at day 14 and 28 suggests that cell death was a consequence of apoptosis (Figure 4C,D; Supplementary Figure S3). Importantly, when MNs are cultured in absence of muscle cells, we did not observe differences in CC-3 signal among the 3 genotypes (Figure 4D).
To confirm these observations in an independent pair of isogenic FUS lines, we introduced the P525L variant in another iPSC line (EBiSC catalogue number WTSIi004-A, male, age of donor 35-39) (Supplementary Figure S4A). In these lines, hereafter named WTSI-FUS^{WT} and WTSI-FUS^{P525L}, we confirmed upregulation of HuD in FUS mutant MNs (Supplementary Figure S4B). Moreover, when co-cultured with FUS^{WT} SkMCs, we observed reduction in muscle fibers forming endplates and increased apoptosis in presence of WTSI-FUS^{P525L} MNs, compared with the co-cultures obtained with isogenic WTSI-FUS^{WT} MNs (Supplementary Figure S4C,D; Supplementary Figure S5A,B). We then produced a WTSI-FUS^{WT} line containing the Syn1:HuD transgene (hereafter WTSI-FUS^{WT}+HuD). Also in this case, HuD overexpression resulted in a significant reduction of muscle fibers forming NMJs and increase in apoptosis (Supplementary Figure S4C,D; Supplementary Figure S5A,B).
Collectively, these results show that, in addition to NMJ formation impairment, HuD overexpression in MNs closely phenocopies the severe FUS P525L ALS variant in terms of increased vulnerability by apoptosis, and that such effect emerges only in presence of muscle cells.

Knockdown of HuD or its target genes in FUS^{P525L} co-cultures rescues NMJ defects and apoptosis

Since the effects of HuD overexpression in MNs are strikingly similar to those exerted by the FUS^{P525L} variant, we wondered whether reduction of HuD levels could be beneficial for NMJ formation and survival in co-cultures made by FUS^{P525L} MNs. Small interfering RNAs (siRNAs) transfection effectively reduced HuD mRNA levels in FUS^{P525L} MNs (Supplementary Figure S6A). Co-cultures of FUS^{WT} SkMCs and FUS^{P525L} MNs were transfected at day 3 and 8 with anti-HuD siRNAs and analyzed at day 14 by αBTX and CC-3 staining. This analysis revealed significant increase in the fraction of muscle fibers showing AChR clusters and significant reduction of apoptosis upon HuD knockdown (Figure 5A-D; Supplementary Figure S6B,C). The same effects were consistently observed upon HuD siRNAs transfection in co-cultures made of WTSI-FUS^{P525L} MNs (Supplementary Figure S7A,B). We next performed a similar experiment by knocking down, individually, two key HuD targets, NRN1 and GAP43, whose levels are increased in FUS^{P525L} MNs due to overly stabilization by HuD (Supplementary Figure S6A; Garone et al., 2021). NRN1 siRNAs significantly increased the fraction of muscle fibers showing AChR clusters, but to lesser extent compared to HuD knockdown, while their effect on apoptosis was comparable (Figure 5A-D; Supplementary Figure S6B,C). GAP43

knockdown did not significantly change AChR clustering and produced a milder effect on apoptosis.
Taken together these results suggest that most, if not all, the cell-autonomous effects of the FUS^{P525L} variant in MNs in terms of NMJ defects and apoptosis could be due to HuD upregulation. In turn, among the tested HuD targets that are also upregulated in FUS mutant MNs (Garone et al., 2021), NRN1 might play a prominent role.

Knockdown of the Drosophila HuD ortholog *elav* rescues the motor dysfunction caused by FUS overexpression *in vivo*

Drosophila models represent valuable tools for examining genetic modifiers of neurodegenerative diseases, including FUS-ALS (Casci and Pandey, 2015). In *Drosophila melanogaster*, the neuronal *embryonic lethal abnormal vision* (*elav*) gene encodes for an RBP, ELAV, showing high conservation with the mammalian HuD protein in terms of structure, expression and functions (Bronicki and Jasmin, 2013). We took advantage of fly models selectively overexpressing human FUS WT or P525L in neurons, which show reduced climbing ability (Marrone et al., 2019), to assess whether *elav* modulation might modify such motor dysfunction phenotype. Upon ELAV overexpression in neurons, we observed a strong reduction in the number of flies able to cross a 4cm threshold in a climbing assay performed at day 6 (Figure 6A). At this age, neither WT nor P525L FUS overexpression resulted in motor dysfunction. At day 15, overexpression of ELAV strongly worsened the motor phenotypes in FUS expressing animals (Figure 6B). Notably, at this time point, the FUS P525L animals with ELAV overexpression died due to strong phenotype/toxicity, whereas animals expressing FUS P525L alone were still alive with strong motor dysfunction. We then attempted a rescue experiment at an intermediate time point, 11 days, when WT or P525L FUS overexpression reduced to about 50% the fraction of flies able to perform the climbing assay. ELAV levels reduction by neuronal-specific expression of short hairpin RNAs (shRNAs) produced per se a mild motor phenotype dysfunction in normal flies. Strikingly, *elav* shRNAs significantly rescued the motor dysfunction for both WT and P525L FUS (Figure 6C,D).
Collectively, in line with the results from the *in vitro* human model, these *in vivo* experiments in *Drosophila* show that overexpression of the HuD-related protein ELAV produces *per se* motor dysfunction and exacerbates the effects of FUS expression, whereas ELAV dampening is sufficient to rescue the motor phenotype produced by FUS completely.

HuD transcription is induced by oxidative stress in human MNs

Our previous work showed increased HuD levels in FUS mutant human iPSC-derived MNs and in the spinal cord of a FUS mutant mouse model (Garone et al., 2021). We and others have also previously detected HuD in pathological aggregates of FUS, TDP-43 and sporadic ALS (sALS) patients (Blokhuis et al., 2016; De Santis et al., 2019). More recently, the Cereda lab reported HuD overexpression in sALS patients' motor cortex and proposed that this could be due to induction of HuD expression upon oxidative stress, as HuD mRNA levels were increased in neuroblastoma cells treated with H_2O_2 (Dell'Orco et al., 2021). These findings prompted us to assess whether the same effect could be observed in human MNs. MNs from FUS^{WT} iPSCs were treated with sodium arsenite, an inducer of oxidative stress, for 60 minutes before mRNA analysis by qRT-PCR. We found a small but highly reproducible increase of *HuD*

transcript levels upon oxidative stress (Figure 7A). We observed a similar effect in FUS^{WT} iPSC-derived co-cultures (Figure 7B). Upregulation of HuD was likely due to new transcription, as pre-treatment with α-amanitin abolished the effect of oxidative stress on this transcript (Figure 7C). All these results were confirmed in WTSI-FUS^{WT} MNs and co-cultures (Figure 7D-E). Together with the previous findings (Dell'Orco et al., 2021), these results suggest that oxidative stress might trigger HuD expression increase in human neurons, including MNs, with possible implications for sALS. To investigate this possibility, we took advantage of a large transcriptome profiling dataset of sALS patients (Tam et al., 2019). In this dataset, ALS patients' cortex samples could be grouped into 3 distinct clusters based on expression profile. The largest group included patients with hallmarks of oxidative and proteotoxic stress (ALS_Ox). The other two clusters showed signatures of glial activation (ALS_Glia) and high retrotransposon expression (ALS_TE) (Tam et al., 2019). Notably, we found that HuD expression was significantly increased only in the ALS_Ox cluster (Figure 7G). Conversely, its levels were significantly lower in the ALS_Glia group and no significant change was found in ALS_TE group. This pattern was also evident for the HuD targets, NRN1 (albeit its increase in ALS_Ox did not reach statistical significance) and GAP43 (Figure 7G). Moreover, the ELAV family member *ELAVL2*, encoding for an RBP (HuB) closely related to HuD, also showed significant increased expression in ALS_Ox, decreased expression in ALS_Glia and no change in ALS_TE (Supplementary Figure S8A). Finally, *SOD1* mRNA, which is a target stabilized by HuD upon oxidative stress (Dell'Orco et al., 2021), was also significantly upregulated in the ALS_Ox group (Supplementary Figure S8A).
These findings suggest that, in the absence of pathogenic FUS ALS variants, oxidative stress can trigger HuD upregulation in the context of human MNs *in vitro*. Accordingly, HuD levels are specifically increased in sALS patients with a signature related to oxidative stress.

DISCUSSION

Human *in vitro* models of the motor unit have shown that MN-restricted expression of ALS-linked FUS variants produces NMJ phenotypes (Picchiarelli et al., 2019; Stoklund Dittlau et al., 2021). Here we found that such NMJ defects could be reverted by dampening HuD levels. Moreover, knockdown of HuD decreased mutant FUS-induced apoptosis *in vitro* and, strikingly, knockdown of the related *elav* Drosophila gene completely rescued motor phenotypes induced by FUS *in vivo*. We have recently shown that in MNs FUS mutation or HuD overexpression exert similar effects in the expression of disease-linked genes (Garone et al., 2023). Altogether, these findings point to a crucial role for HuD in the cell autonomous mechanisms that underlie the death of MNs via a "dying back" pattern in FUS and, possibly, a subset of sporadic ALS cases with hallmarks of oxidative and proteotoxic stress.
The seminal discovery of early defects at the NMJ in 47-days old $SOD1^{G93A}$ mice, in which loss of MNs occurs only after 90 days of age, supported the "dying back" hypothesis which was further reinforced by evidence from a sALS patient and other non-SOD1 ALS animal models (Fischer et al., 2004; Alhindi et al., 2021). These include the $Fus^{\Delta NLS/+}$ mice that show reduced endplate area and NMJ denervation as early as 1 month of age, while motor deficits begin around 10 months and MN loss was evident only at 22 months (Scekic-Zahirovic et al., 2017;

Picchiarelli et al., 2019). Neuron-specific expression of mutant human FUS proteins driven by the *MAPT* regulatory sequences also resulted in early structural and functional defects at the NMJ that preceded MN loss (Sharma et al., 2016). These phenotypes were particularly severe in the MAPT-hFUS^{P525L} mouse, which showed significant denervation at day 20 and MN loss at day 30. This evidence suggests that MN-restricted expression of mutant FUS is sufficient *in vivo* to trigger early retraction of motor axons from the NMJ. Since HuD upregulation was observed in mice carrying a severe FUS mutation in the NLS (Fus-Δ14 knock-in) (Garone et al., 2021), we can speculate that the HuD-dependent circuitry described here could contribute to such NMJ defects due to pre-synaptic mechanisms. The evidence of HuD upregulation in the motor cortex of sporadic ALS patients, possibly due to exposure to environmental factors causing oxidative stress (Dell'Orco et al., 2021), suggests that this RBPs might play a broader role in ALS. To this regard, we and others have previously found HuD in cytoplasmic inclusions of FUS, TDP-43 and sporadic ALS patients (Blokhius et al., 2016; De Santis et al., 2019). In this work we further explored the possibility that HuD might be altered in sporadic ALS. We found increased levels of HuD and some of its targets in a subset of sporadic ALS patients characterized by a signature related to oxidative stress, who account for the largest subgroup (about 60% of the cohort) (Tam et al., 2019). Intriguingly, a significant decrease was instead observed in the cluster with a signature related to glial activation and inflammation (about 20% of the cohort). Thus, taken together, altered HuD levels in either direction would be associated with most sporadic ALS cases. Here we show that *HuD* mRNA levels increase upon oxidative stress is likely due to transcriptional regulation. So far, to the best of our knowledge, no known genetic variants in the *HuD* gene have been conclusively linked to ALS. However, from a survey of the Project MinE (http://databrowser.projectmine.com) we noticed 4 variants of uncertain significance (VUS) found in ALS patients but not in controls (Supplementary Figure 8C,D). Future work will be needed to clarify if such VUS have any effect on HuD protein levels and/or activity.

Among known HuD targets, in this work we focused on NRN1 and GAP43. Notably, in postmortem ALS patients both GAP43 and NRN1 have been found upregulated in regions of the nervous system with implications in ALS and frontotemporal lobar degeneration (FTLD), including the anterior horn of the spinal cord and the frontal cortex area 8 (Parhad et al., 1992; Ikemoto et al. 1999; Andrés-Benito et al., 2017). This is in line with the known role of HuD in stabilizing (and localizing) GAP43 and NRN1 mRNAs through AU-rich elements (ARE) (Wang et al., Neurochem. Res. 2011; Yoo et al., 2013). We found that knockdown of NRN1 or GAP43 produced a partial rescue of NMJ and/or apoptosis phenotypes in co-cultures containing FUS mutant MNs. This effect might be due to their known roles in developing neurons. To this regard, aberrant axon guidance is among the proposed mechanisms underlying the "dying back" phenomenon (Pasterkamp and Giger, 2009; Dadon-Nachum et al., 2011). For instance, it has been shown that increased expression of the axon guidance protein Semaphorin 3A (Sema3A) by terminal Schwann cells (tSCs) might result in axonal denervation at the NMJ due to repulsion of the motor axon in SOD1^{G93A} mice (de Winter, 2006). Notably, GAP43 can modulate axon guidance signals triggered by Sema3A, and exposure to Sema3A induced neuronal death by apoptosis in a GAP43-dependent manner (Gagliardini et al., 2000). Accordingly, loss of GAP43 conferred resistance to apoptotic stimuli in cultured mouse neurons. On the other hand, overexpression of GAP43 in adult mice resulted in prolonged

sprouting and death of MNs (Aigner et a., 1995; Harding et al., 1999). In line with these studies in animal models, we show here that knockdown of GAP43 by RNAi partially reverts apoptosis in iPSC-derived co-cultures made by mutant FUS MNs. In this case, however, we speculate that increased HuD levels would mediate GAP43 gain of function in a cell autonomous manner, rather than by Sema3A signaling, as our in vitro model does not contain tSCs.
We found that NRN1 knockdown in FUS mutant MNs increased AChR clusters. Previous literature on a possible role for NRN1 in NMJ formation is scarce. A relevant study in *Xenopus laevis* tadpoles showed that overexpression of the ortholog gene *cpg15* promoted spinal MN axon growth by increasing branch addition and maintenance and decreasing branch retraction (Javaherian and Cline, 2005). This dysregulation could eventually impact some crucial processes such as extension, refinement, and pruning. Indeed, in such developmental context, new branches formed upon *NRN1*/*cpg15* overexpression were apposed to AChR clusters. However, the authors did not provide information on further maturation of the new endplates, and whether increased branching during development would be followed by productive formation of mature NMJs remains unclear. It should be noted that the adult human spinal cord is among the nervous system districts with the lowest expression of *NRN1* (Garone et al., 2021). We might speculate that aberrantly increased levels of this growth promoting factor might be detrimental, rather than beneficial, in the adult motor system, generating excess of axonal extensions, which would be less able to establish functional connections.
The case of the sporadic ALS patient who died unexpectedly (Fischer et al., 2004), despite anecdotal, suggests that at the time of diagnosis (first signs of motor symptoms) MN cell bodies might still be intact. Thus, early intervention aimed to restore NMJs might result in an effective therapeutic approach to prevent irreversible subsequent MN degeneration. To this regard, our work shows that individual knockdown of HuD and two of its key target genes, NRN1 and GAP43, can rescue endplate formation and apoptosis in vitro. Moreover, *in vivo* evidence from the Drosophila model shows that reduction of the *HuD*-related gene *elav* expression is sufficient to rescue the motor phenotype caused by FUS completely. Here we took advantage of RNA interference. However, recent advances in the development of antisense oligonucleotides (ASOs) for therapy, also in the context of ALS (McCampbell et al., 2018), provide the opportunity to translate these findings to patients in the near future.

MATERIALS AND METHODS

iPSC culture, transfection and differentiation

Human iPSC lines were maintained in Nutristem-XF medium (Biological Industries), with 0.1X Penicillin/Streptomycin (Merck Life Sciences) (Nutristem P/S), in Matrigel-coated dishes (hESC-qualified Matrigel; Corning) and passaged every 4-5 days with 1 mg/ml Dispase (Gibco). Human isogenic FUS^{WT}, FUS^{P525L} and FUS^{WT}+HuD iPSC lines, all derived from the WT-I line (Lenzi et al., 2015), were previously generated and characterized (Garone et al., 2021). The FUS^{WT} iPSCs line WTSIi004-A (WTSI-FUS^{WT}) was obtained by the European Bank for induced pluripotent Stem Cells (EBiSC). From these cells we generated the isogenic WTSI-FUS^{P525L} iPSC line by TALEN-directed mutagenesis as previously described (Lenzi et al., 2015). To generate the iPSC line WTSI-FUS^{WT} overexpressing HuD (WTSI-FUS^{WT}+HuD), cells

were co-transfected with 4.5 µg of transposable vector epB-Puro-TT-SYN1-HuD (SYN1::HuD) and 0.5 µg of the piggyBac transposase using the Neon Transfection System (Life Technologies) as described (Garone et al., 2021). Stable and inducible iPSCs for spinal MN differentiation (NIL iPSCs) were obtained as previously described (De Santis et al., 2018; Garone et al., 2019). Briefly, iPSCs were transfected with 4.5 µg of NIL piggyBac construct and 0.5 µg of transposase vector using the Neon Tranfection System (Life Technologies) and then selected with 5 µg/ml blasticidin in Nutristem-XF medium containing 0.1X P/S for 10 days. KOLF-1 (FUS^{WT}) iPSCs, stably transfected with inducible transposable vectors encoding for BAF60c and MyoD1 (Tiago et al., 2021) (MB iPSCs), were used to generate SkMCs. Briefly, this line was generated by co-transfecting iPSCs with 2.25 µg each of the ePB-Bsd-TT-BAF60c and ePB-Puro-TT-m-MyoD vectors, and 0.5 µg of piggyBac transposase, and then selected with 1 µg/ml puromycin and 5µg/ml blasticidin in Nutristem P/S for 10 days, as previously described (Lenzi et al., 2016)

Differentiation of spinal MNs and SkMCs and co-cultures

Spinal MNs were obtained as previously described (De Santis et al., 2018; Garone et al., 2019). Briefly, NIL iPSCs were dissociated with Accutase (Thermo Fisher Scientific) to single cells and replated in Nutristem P/S supplemented with 10 µM Y-27632 ROCK inhibitor (Enzo Life Sciences). The next day differentiation was induced in DMEM/F12 (Dulbecco's Modified Eagle's Medium/ Nutrient Mixture F-12 Ham; Merck Life Sciences), 1X Glutamax (Thermo Fisher Scientific), 1X NEAA (Thermo Fisher Scientific), 0.5X P/S and doxycycline 1 µg/ml (Thermo Fisher Scientific) for 2 days. On the third day, medium was replaced by Neurobasal/B27 (Neurobasal medium, Thermo Fisher Scientific; 1X B27, Thermo Fisher Scientific; 1X Glutamax; 1X NEAA; 0.5X P/S) supplemented with 5 µM DAPT, 4 µM SU5402 (both from Merck Life Sciences) and 1 µg/ml doxycycline for 3 days. At day 5, MN progenitors were dissociated with Accutase and counted. $1x10^6$ cells were plated onto Matrigel-coated 35 mm dishes for RNA analyses, and $5x10^4$ cells per well were plated onto Matrigel-coated µ-Slide 8 Well (ibidi) for immunofluorescence analyses. 10 µM of Y-27632 ROCK inhibitor was added for 24h after dissociation. Neurons were maintained in Neurobasal/B27 supplemented with 20 ng/ml L-ascorbic acid (Merck Life Sciences), 20 ng/ml BDNF (PreproTech) and 10 ng/ml GDNF (PreproTech).

To obtain SkMCs, MB iPSCs were dissociated with Accutase (Thermo Fisher Scientific) to single cells and replated in Nutristem P/S supplemented with 10 µM Y-27632 in 35 mm dishes ($2x10^5$ cells). In the following two days, cells were maintained with Growth Medium consisting of high glucose DMEM (Merck Life Sciences), 1X Glutamax, 1X P/S, 20% FBS (Merck Life Sciences), 50 µg/ml Insulin (Roche), 25 ng/ml bFGF (Corning) and 10 ng/ml hEGF (Corning) and 200 ng/ml doxycycline. At day 2, medium was replaced by Skeletal Muscle Differentiation Medium (Promega), 1X P/S, 200 ng/ml doxycycline and 2µM Ara-C (Merck Life Sciences). At day 4, this medium was replaced by Skeletal Muscle Differentiation Medium, 1X P/S and 200 ng/ml doxycycline. The medium was then changed every other day.

To generate co-cultures of spinal MNs and SkMCs we adapted previously published protocols (Guo et al., 2011; Stoklund Dittlau et al., 2021). MB iPSCs were dissociated and replated in 35 mm dishes ($2x10^5$ cells) or µ-Slide 8 Well ($2x10^4$ cells per well) and then SkMC differentiation was induced as described above. Spinal MNs differentiation started independently and in

parallel when SkMCs were at day 7 of the muscle differentiation protocol. At day 5, MNs progenitors were replated (at approximately 1:1 ratio) in the 35mm dishes ($5x10^5$ cells) or μ-Slide 8 Well ($5x10^4$ cells per well) containing SkMCs, which at this stage had reached day 13 of differentiation, in Neurobasal/B27 medium containing 20 ng/ml L-ascorbic acid, 20 ng/ml BDNF, 10 ng/ml GDNF, 200 ng/ml doxycycline and 10 μM Y-27632. The next day, medium was replaced with Neurobasal/B27, 20 ng/ml L- ascorbic acid, 20 ng/ml BDNF, 10 ng/ml GDNF, 200 ng/ml doxycycline, 20 μg/ml laminin (Merck Life Sciences) and 0.01 μg/ml agrin (R&D system). Co-cultures were maintained for 14, 28 or 50 days, changing medium every 4 days.

Functional assays

Functional activity in co-cultures and muscle monocultures was assessed by adding 50μM glutamate (Gibco) to cells previously plated in μ-Slide 8 Well supports and maintained in Neurobasal/B27 medium containing 20 ng/ml L-ascorbic acid, 20 ng/ml BDNF and 10 ng/ml GDNF. The number of muscle contractions per minute was counted under Carl Zeiss Axio Vert.A1 Microscope. To verify muscle contraction inhibition, 10μM tubocurarine (Sigma-Aldrich) was added to the medium containing glutamate. The same co-culture region was identified for measuring muscle contractions per minute.

Real-Time qRT-PCR

Total RNA was extracted using E.Z.N.A Total RNA Kit I (Omega BIO-TEK) and retrotranscribed with iScript Supermix (Bio-Rad Laboratories) according to manufacturers' instructions. qRT-PCR was performed with the iTaq Universal SYBR Green Supermix kit (Bio-Rad Laboratories) on a ViiA 7 system (Thermo Fisher Scientific). *ATP5O* and *TUBB3* were employed as calibrator genes. Full list of primers is reported in Supplementary Table S1.

Immunofluorescence and confocal imaging

Cells were fixed in 4 % PFA (Electron microscopy sciences) and 30 mM sucrose (Sigma-Aldrich) for 10 min at room temperature (RT), then washed with PBS with calcium chloride and magnesium chloride (Merck Life Sciences) and permeabilized with a solution of 0.5% BSA, 10% Horse Serum (HRS), 0.2% Triton X-100 and PBS (Merck Life Sciences) for 15 min. Cells were then washed and treated with a blocking solution composed of 0.5% BSA, 10% HRS and PBS for 30 min. For NMJ staining, anti-MyHC (1:50; MAB4470, R&D system) was diluted in blocking solution and incubated at 4°C overnight. anti-TUJ1 (1:1000; T2200, Merck Life Sciences) was diluted in the same solution and incubated for 1 h at RT. Cells were then washed with PBS and incubated with α-bungarotoxin-488 (1:350, B13422, Thermo Fisher Scientific) for 1 h at RT. Secondary anti-mouse Alexa Fluor 647 (1:250, Immunological Science) and anti-rabbit Alexa Fluor 594 (1:250, Immunological Sciences) antibodies were then incubated for 1 h. DAPI (1:2000; Sigma-Aldrich) diluted in 0.5% BSA, 10% HRS in PBS was added for 5 minutes. Cells were washed in PBS and ibidi Mounting Medium (50001, ibidi) was added. Confocal image stacks were acquired using an inverted Olympus iX73 equipped with an X-light V3 spinning disc head (Crest Optics), a LDI laser illuminator (89 North), Prime BSI sCMOS camera (Photometrics) and MetaMorph software (Molecular devices) with 40X air or 100X oil objectives (Olympus). For skeletal muscle with or without 48 h Ara-C treatment, fixed cells were incubated with anti-MyHC (1:50; MAB4470, R&D system) and anti-NANOG (1:200; PA1-

097X; Thermo Fisher Scientific) primary antibodies overnight. Then, anti-mouse Alexa Fluor 647 (1:250, Immunological Science), anti-rabbit Alexa Fluor 488 (1:250, Immunological Science) and DAPI were used and mounted with ibidi Mounting Medium (50001, ibidi). Confocal image stacks were acquired using an Olympus FV1200 confocal laser scanning microscope with 20X air-objective.

Cell-based assays and confocal imaging

For apoptosis analysis, fixed cells were incubated with anti-CC3 (1:400, 9661, Cell signaling) overnight, anti-MAP2 (1:2000, ab5392, Abcam) for 1h at RT. Anti-chicken Alexa Fluor 488 (1:250, Immunological Sciences) and anti-rabbit Alexa Fluor 594 (1:250, Immunological Sciences) secondary antibodies were then used. DAPI was added for 5 minutes. Confocal image stacks were acquired using an Olympus FV10i laser scanning confocal microscope with 10X air objective at 2x zoom or the X-light V3 spinning disc confocal microscope described before with 20X air objective (Olympus). Phase-contrast images were acquired using Carl Zeiss Axio Vert.A1 Microscope with 20X or 40X air objectives. For dead cell quantification, live co-cultures were incubated (5% CO_2 at 37°C) with Neurobasal/B27, 20 ng/ml L-ascorbic acid, 20 ng/ml BDNF and 10 ng/ml GDNF medium supplemented with 0.6 µl ethidium homodimer-1 594 (Thermo Fisher Scientific) according to manufacturer's protocol. After 30 minutes cells were washed with PBS and maintained in Neurobasal/B27, 20 ng/ml L-ascorbic acid, 20 ng/ml BDNF and 10 ng/ml GDNF medium during acquisition. Confocal image stacks were acquired using Olympus FV10i laser scanning confocal microscope with 10x air objective at 1.5x zoom.

RNA interference (RNAi) iPSC-derived in co-cultures

Lyophilized siRNAs were resuspended in nuclease-free water at 20µM stock concentration. HuD, NRN1, GAP-43 and non-targeting siRNAs (siRNA-SMARTpool and ON-TARGET plus Non-targetingPool, Dharmacon) were transfected at 10 nM concentration using siLentFect Lipid Reagent (Bio-Rad Laboratories) according to manufacturer's instructions. Medium was replaced 5 h after transfection.

***Drosophila melanogaster* stocks**

All *Drosophila* crosses were maintained on standard cornmeal medium at 25°C in light/dark-controlled incubators. The UAS-FUS WT and UAS-FUS P525L lines were generated through site specific insertion of the transgene at BestGene Inc. using the (attp2) integration vector and were previously described (Casci et al., 2019; Anderson et al., 2018). The TRIP control lines, UAS-Luciferase (LUC OE, # 35789) and UAS-Luciferase RNAi (LUC RNAi, # 31603) were obtained from Bloomington Drosophila Resource Center (BDSC). The UAS-elav RNAi (# 28371) and UAS-elav (ELAV OE, stock # 38400) were also obtained from BDSC. The ElavGS-Gal4 was a kind gift from Dr. Haig Keshishian.

***Drosophila melanogaster* motor function assays**

ELAV-GS (neuron specific driver) was used to express FUS-WT and FUS-P525L with and without overexpression and/or knockdown of ELAV. For performing the climbing assay, flies were crossed in the absence of RU486 (mifepristone, Cayman Chemical, #10006317) on standard food. Day 1 female adult *Drosophila* were transferred to RU486 (5mM) drug food and

placed in 25°C before performing the motor function assay at the time points indicated. Flies were transferred to empty rounded vials and were allowed to acclimatize for 15 minutes in the new vials. Flies were knocked to the bottom of the vials by tapping each vial against the laboratory bench three times, and a video camera was used to record flies climbing up the walls. The percentage of flies that climbed 4cm in 10s of each individual fly was quantified and analyzed using GraphPad PRISM 8.0 software. Three experimental replicates were performed for each group.

Oxidative stress induction and transcription block

Cells were left untreated or treated with 0.5 mM sodium arsenite (Merck Life Sciences) to induce acute oxidative stress for 1h. For transcription inhibition, 25 µl/ml α-amanitin solution (Merck Life Sciences) was added to the medium for 8h; in the last hour, 0.5 mM sodium arsenite was added to induce oxidative stress.

Bioinformatics analysis of sporadic ALS RNA-seq datasets

The raw count matrix relative to the RNA-seq analysis of ALS patient samples and individuals with and without other neurological disorders produced by the NYGC consortium (Tam et al., 2019) was retrieved from the Gene Expression Omnibus (GEO) database (Edgar et al., 2002) (accession number: GSE124439), while the metadata information was taken from the original publication. Starting from this matrix, sample-specific gene-level FPKM (Fragments Per Kilobase of exon per Million mapped reads, a normalized expression measure) values were calculated using the “fpkm” function from the DESeq2 v1.32.0 R package (Love et al., 2014) and the exonic gene size information retrieved from the GENCODE v42 annotation (Harrow et al., 2012). Differential expression analysis between different conditions was performed using the “DESeq” function, controlling for sex and tissue type.

Statistics and reproducibility.

Statistical analysis, graphs, and plots were generated using GraphPad PRISM 6.0 or 8.0 (GraphPad Software). The statistical test used is indicated in each figure legend. Sample size and the definition of replicates for each experiment is also indicated in the figure legends. *p* values are indicated in the figures.

DATA AVAILABILITY

All data generated or analyzed during this study are included in the manuscript and supporting files. Materials are available upon request.

AUTHOR CONTRIBUTION

Conceptualization, B.S., A.R.; Formal analysis, B.S., M.M., D.M., A.C.; Investigation, B.S., D.M.; Methodology, B.S., M.M., A.C., B.B., V.d.T., M.G.G.; Project administration, A.R.; Supervision, U.B.P., A.R.; Writing - original draft, A.R.; Writing - Review & Editing, B.S., U.B.P., A.R.. All authors read and approved the final manuscript.

ACKNOWLEDGEMENTS

The authors wish to thank the Imaging Facility at Center for Life Nano and Neuro-Science, Fondazione Istituto Italiano di Tecnologia, for support and technical advice. We thank Dr. Tiziana Santini and Dr. Ersilia Fornetti for advice on NMJ staining and analysis. We thank Dr. R. De Santis, Prof. I. Bozzoni, prof. S. Di Angelantonio and the members of the Rosa lab for helpful discussion.
Project funded under the National Recovery and Resilience Plan (NRRP), Mission 4, Component 2, Investment 1.4 - funded by the European Union - NextGenerationEU - CN00000041 - CUP: B83C22002870006 - to AR.

COMPETING INTERESTS

The authors declare no competing interests.

REFERENCES

Aigner, L. et al. Overexpression of the neural growth-associated protein GAP-43 induces nerve sprouting in the adult nervous system of transgenic mice. Cell 83, 269–278 (1995).

Alhindi, A., Boehm, I. & Chaytow, H. Small junction, big problems: Neuromuscular junction pathology in mouse models of amyotrophic lateral sclerosis (ALS). J Anat (2021). doi:10.1111/joa.13463

Anderson, E. N. et al. Traumatic injury induces stress granule formation and enhances motor dysfunctions in ALS/FTD models. Hum Mol Genet 27, 1366–1381 (2018).

Andrés-Benito, P., Moreno, J., Aso, E., Povedano, M. & Ferrer, I. Amyotrophic lateral sclerosis, gene deregulation in the anterior horn of the spinal cord and frontal cortex area 8: implications in frontotemporal lobar degeneration. Aging (Albany NY) 9, 823–851 (2017).

Blokhuis, A. M. et al. Comparative interactomics analysis of different ALS-associated proteins identifies converging molecular pathways. Acta Neuropathol 132, 175–196 (2016).

Bronicki, L. M. & Jasmin, B. J. Emerging complexity of the HuD/ELAVl4 gene; implications for neuronal development, function, and dysfunction. RNA 19, 1019–1037 (2013).

Brown, R. H. & Al-Chalabi, A. Amyotrophic Lateral Sclerosis. N Engl J Med 377, 162–172 (2017).

Caputo, L. et al. Acute conversion of patient-derived Duchenne muscular dystrophy iPSC into myotubes reveals constitutive and inducible over-activation of TGFβ-dependent pro-fibrotic signaling. Skelet Muscle 10, 642 (2020).

Casci, I. et al. Muscleblind acts as a modifier of FUS toxicity by modulating stress granule dynamics and SMN localization. Nat Commun 10, 5583 (2019).

Casci, I. & Pandey, U. B. A fruitful endeavor: modeling ALS in the fruit fly. Brain Res 1607, 47–74 (2015).

Dadon-Nachum, M., Melamed, E. & Offen, D. The ‘dying-back’ phenomenon of motor neurons in ALS. Journal of molecular neuroscience : MN 43, 470–477 (2011).

Dassi, E. Handshakes and Fights: The Regulatory Interplay of RNA-Binding Proteins. Front Mol Biosci 4, 67 (2017).

Dell'Orco, M. et al. HuD regulates SOD1 expression during oxidative stress in differentiated neuroblastoma cells and sporadic ALS motor cortex. Neurobiology of Disease 148, 105211 (2021).

Edgar, R., Domrachev, M. & Lash, A. E. Gene Expression Omnibus: NCBI gene expression and hybridization array data repository. Nucleic Acids Res 30, 207–210 (2002).

Fischer, L. R. et al. Amyotrophic lateral sclerosis is a distal axonopathy: evidence in mice and man. Exp Neurol 185, 232–240 (2004).

Gagliardini, V., Dusart, I. & Fankhauser, C. Absence of GAP-43 can protect neurons from death. Mol Cell Neurosci 16, 27–33 (2000).

Garone, M. G. et al. Conversion of Human Induced Pluripotent Stem Cells (iPSCs) into Functional Spinal and Cranial Motor Neurons Using PiggyBac Vectors. J Vis Exp (2019). doi:10.3791/59321

Garone, M. G. et al. Proteomics analysis of FUS mutant human motoneurons reveals altered regulation of cytoskeleton and other ALS-linked proteins via 3'UTR binding. Sci Rep 10, 11827 (2020).

Garone, M. G. et al. ALS-related FUS mutations alter axon growth in motoneurons and affect HuD/ELAVL4 and FMRP activity. Commun Biol 4, 1025 (2021).

Garone, M. G., Salerno, D. & Rosa, A. Digital color-coded molecular barcoding reveals dysregulation of common FUS and FMRP targets in soma and neurites of ALS mutant motoneurons. Cell Death Discov 9, 33 (2023).

Guo, X., Gonzalez, M., Stancescu, M., Vandenburgh, H. H. & Hickman, J. J. Neuromuscular junction formation between human stem cell-derived motoneurons and human skeletal muscle in a defined system. Biomaterials 32, 9602–9611 (2011).

Harding, D. I., Greensmith, L., Mason, M., Anderson, P. N. & Vrbová, G. Overexpression of GAP-43 induces prolonged sprouting and causes death of adult motoneurons. Eur J Neurosci 11, 2237–2242 (1999).

Harrow, J. et al. GENCODE: the reference human genome annotation for The ENCODE Project. Genome Res 22, 1760–1774 (2012).

Ichikawa, N. et al. Identification of neurite outgrowth active sites on the laminin alpha4 chain G domain. Biochemistry 44, 5755–5762 (2005).

Ikemoto, A., Hirano, A. & Akiguchi, I. Increased expression of growth-associated protein 43 on the surface of the anterior horn cells in amyotrophic lateral sclerosis. Acta Neuropathol 98, 367–373 (1999).

Javaherian, A. & Cline, H. T. Coordinated motor neuron axon growth and neuromuscular synaptogenesis are promoted by CPG15 in vivo. Neuron 45, 505–512 (2005).

Lenzi, J. et al. Differentiation of control and ALS mutant human iPSCs into functional skeletal muscle cells, a tool for the study of neuromuscolar diseases. Stem Cell Research 17, 140–147 (2016).

Lenzi, J. et al. ALS mutant FUS proteins are recruited into stress granules in induced Pluripotent Stem Cells (iPSCs) derived motoneurons. Dis Model Mech 8, 755–766 (2015).

Love, M. I., Huber, W. & Anders, S. Moderated estimation of fold change and dispersion for RNA-seq data with DESeq2. Genome Biol. 15, 550 (2014).

Marrone, L. et al. FUS pathology in ALS is linked to alterations in multiple ALS-associated proteins and rescued by drugs stimulating autophagy. Acta Neuropathol (2019). doi:10.1007/s00401-019-01998-x

McCampbell, A. et al. Antisense oligonucleotides extend survival and reverse decrement in muscle response in ALS models. J Clin Invest 128, 3558–3567 (2018).

Parhad, I. M., Oishi, R. & Clark, A. W. GAP-43 gene expression is increased in anterior horn cells of amyotrophic lateral sclerosis. Annals of neurology 31, 593–597 (1992).

Pasterkamp, R. J. & Giger, R. J. Semaphorin function in neural plasticity and disease. Curr Opin Neurobiol 19, 263–274 (2009).

Picchiarelli, G. et al. FUS-mediated regulation of acetylcholine receptor transcription at neuromuscular junctions is compromised in amyotrophic lateral sclerosis. Nature Publishing Group 22, 1793–1805 (2019).

De Santis, R. et al. Mutant FUS and ELAVL4 (HuD) Aberrant Crosstalk in Amyotrophic Lateral Sclerosis. Cell Rep 27, 3818–3831.e5 (2019).

De Santis, R. et al. Direct conversion of human pluripotent stem cells into cranial motor neurons using a piggyBac vector. Stem Cell Research 29, 189–196 (2018).

De Santis, R. et al. FUS Mutant Human Motoneurons Display Altered Transcriptome and microRNA Pathways with Implications for ALS Pathogenesis. Stem Cell Reports 9, 1450–1462 (2017).

Scekic-Zahirovic, J. et al. Motor neuron intrinsic and extrinsic mechanisms contribute to the pathogenesis of FUS-associated amyotrophic lateral sclerosis. Acta Neuropathol 133, 887–906 (2017).

Scekic-Zahirovic, J. et al. Toxic gain of function from mutant FUS protein is crucial to trigger cell autonomous motor neuron loss. EMBO J (2016). doi:10.15252/embj.201592559

Sharma, A. et al. ALS-associated mutant FUS induces selective motor neuron degeneration through toxic gain of function. Nat Commun 7, 10465 (2019).

Silvestri, B., Mochi, M., Garone, M. G. & Rosa, A. Emerging Roles for the RNA-Binding Protein HuD (ELAVL4) in Nervous System Diseases. Int J Mol Sci 23, (2022).

Stoklund Dittlau, K. et al. Human motor units in microfluidic devices are impaired by FUS mutations and improved by HDAC6 inhibition. Stem Cell Reports (2021). doi:10.1016/j.stemcr.2021.03.029

Tam, O. H. et al. Postmortem Cortex Samples Identify Distinct Molecular Subtypes of ALS: Retrotransposon Activation, Oxidative Stress, and Activated Glia. Cell Rep 29, 1164–1177.e5 (2019).

Tiago, T. et al. Small heat-shock protein HSPB3 promotes myogenesis by regulating the lamin B receptor. Cell Death and Disease 12, 452 (2021).

Wang, Z.-H. et al. HuD regulates the cpg15 expression via the 3'-UTR and AU-rich element. Neurochem. Res. 36, 1027–1036 (2011).

de Winter, F. et al. The expression of the chemorepellent Semaphorin 3A is selectively induced in terminal Schwann cells of a subset of neuromuscular synapses that display limited anatomical plasticity and enhanced vulnerability in motor neuron disease. Mol Cell Neurosci 32, 102–117 (2006).

Yoo, S. et al. A HuD-ZBP1 ribonucleoprotein complex localizes GAP-43 mRNA into axons through its 3' untranslated region AU-rich regulatory element. Journal of neurochemistry 126, 792–804 (2013).

FIGURE LEGENDS

Figure 1. Establishment of iPSCs derived MNs and SkMCs co-cultures and functional analysis of NMJs

(A) Schematic representation of the differentiation protocol to generate co-cultures of spinal MNs and SkMCs. A more detailed SkMC differentiation scheme is shown in Supplementary Figure S1. (B) Phase-contrast image of MNs and SkMCs co-culture derived from FUS^{WT} iPSCs at day 14. Examples of MN cell body and SkMC are indicated by arrows. Scale bar: 20 µm. (C) Immunostaining analysis of co-cultures at the indicated time points. α-BTX (magenta) was used as a AChRs clustering marker, TUJ1 (TUBB3, green) and MyHC (grey) are, respectively, neuronal and muscular markers. DAPI (blue) was used for nuclear staining. Scale bar: 15 µm or 10 µm as indicated. (D) Graph showing the number of contractions per minute of the skeletal muscle fibers in day 50 co-cultures before any treatment, upon glutamate treatment and upon glutamate and tubocurarine treatment. The results of 3 independent co-cultures and 1 monoculture of SkMCs only are shown. Points represent the average contractions per minute from of 3 fields in each experiment and the error bars indicate the standard deviation. Student's t-test (paired; two tails) *p* values indicated in the figure are referred to the average of the 3 co-culture experiments.

Figure 2. NMJ analysis in co-cultures

(A) Schematic representation of co-cultures used for analyses shown in Figures 2-5. (B) Representative images of immunofluorescence staining of day 14 co-cultures using the indicated primary antibodies and α-BTX and DAPI. Scale bar for all panels: 50 µm. (C) The graphs report quantitative analysis of the percentage of α-BTX positive fibers (left) and TUJ1 fluorescence intensity (right), at day 14 and 28 of co-culture. Error bars indicate standard deviation (n=3, Student's t-test; unpaired; two tails).

Figure 3. Endplate maturation analysis in co-cultures

(A) Representative images of immunofluorescence staining of day 14 co-cultures using the MyHC antibody and α-BTX and DAPI. Images show representative endplates that were categorized based on morphology into diffuse puncta, aligned puncta (indicated by arrows) and dense/cluster. Scale bar: 10 µm. (B) The graph shows quantification of endplates categories, as a percentage, from co-cultures obtained with FUS^{WT} SkMCs and FUS^{WT}, FUS^{P525L} or FUS^{WT}+HuD MNs. The results of a blind analysis of 165 (FUS^{WT}), 124 (FUS^{P525L}), and 147 (FUS^{WT}+HuD) total endplates from 3 independent differentiation experiments are shown (Student's t-test; unpaired; two tails).

Figure 4. Cell death analysis

(A) Representative brightfield images of co-cultures at day 28. Scale bar: 20µm. (B) Quantitative analysis of dead cells using ethidium homodimer-1 at day 7, 14, 21, 28 of co-cultures obtained with FUS^{WT} SkMCs and FUS^{WT}, FUS^{P525L} or FUS^{WT}+HuD MNs. The graph shows the average and standard deviation from 3 independent differentiation experiments. *p* values indicated by blue and green lines are relative to the comparison of the FUS^{P525L} and FUS^{WT}+HuD group, respectively, to the FUS^{WT} one (Student's t-test; unpaired; two tails). See

Supplementary Figure S2 for representative images of the cells. (C) Representative merged images of immunofluorescence staining of day 14 co-cultures (left panels) or MN monocultures (right panels) using Cleaved Caspase-3 (CC-3) and MAP2 antibodies, and DAPI. Scale bar: 50µm. Single panels are shown in Supplementary Figure S3. (D) The graphs report quantitative analysis of the CC-3 fluorescence intensity at day 14 (top) and 28 (bottom) of co- or monoculture. Average and standard deviation from 3 independent differentiation experiments is shown. *p* values indicated in the figure are relative to the comparison of the cocultures containing FUS^{P525L} and FUS^{WT}+HuD MNs, respectively, to the FUS^{WT} ones; no significant difference resulted from the comparison of MN monocultures ($p>0.05$; not shown) (Student's t-test; unpaired; two tails).

Figure 5. HuD, NRN1 and GAP43 knockdown in co-cultures containing FUS^{P525L} MNs
(A,B) Representative merged images of day 14 co-cultures obtained with FUS^{WT} SkMCs and FUS^{P525L} MNs transfected with the indicated siRNAs and stained with the indicated antibodies. Scale bar: 50µm. Single panels are shown in Supplementary Figure S6. (C,D) The graphs report quantitative analysis of the percentage of α-BTX positive fibers (left) and CC-3 fluorescence intensity (right), at day 14 of co-culture as in (A,B). Error bars indicate standard deviation (n=3, Student's t-test; unpaired; two tails).

Figure 6. Expression of *Drosophila* HuD ortholog *elav* modifies FUS-mediated motor dysfunction
(A,B) The graphs represent the percentage of flies that climb 4cm in 10s at day 6 and day 15 in wild-type FUS (FUS-WT) or mutant FUS (P525L) overexpressing ELAV (ELAV OE) or Luciferase (LUC OE) control respectively. (C, D) The graphs show percent flies that climb 4cm in 10s and 15s respectively at day 11 in wild-type FUS (FUS-WT) or mutant FUS (P525L) by knocking down ELAV (ELAV RNAi) or Luciferase (LUC RNAi) control (Ordinary one-way ANOVA w/ Fisher's LSD test). n = 6-10 adult flies per genotype. Three experimental replicates were performed for each group. Error bars indicate S.E.M. The asterisks represent difference between groups *p value <0.05; **p value <0.01; ***p value <0.001; ****p value <0.0001

Figure 7. *HuD* expression upon oxidative stress *in vitro* and in sporadic ALS patients
(A,B) The graphs show quantitative analysis of *HuD* mRNA levels in control conditions or upon acute stress treatment with 0.5 mM sodium arsenite (ARS) for 1h in FUS^{WT} iPSCs derived spinal MNs monocultures at day 12 (A) or FUS^{WT} iPSCs derived co-cultures at day 7 (B). (C) Cells as in panel (A) were pre-treated or not with α-amanitin before oxidative stress induction with ARS. (D-F) The experiments shown in panels (A-C) were repeated with the WTSI-FUS^{WT} iPSC line. In panels (A-F) ATP5O expression was used for normalization and the graphs show the average, standard deviation and *p* values from 3 or 4 biological replicates (Student's t-test; unpaired; two tails). (G) Violin plots showing the expression levels, reported as log-transformed FPKM values, of *HuD*, *NRN1* and *GAP43* in post-mortem sporadic ALS patients' cortex samples from (Tam et al., 2019). OND: other neurodegenerative diseases; CTR: healthy individuals; ALS_Glia: sporadic ALS patients with a signature of glial activation; ALS_Ox: sporadic ALS patients with a signature of oxidative and proteotoxic stress; ALS_TE: sporadic

ALS patients with a signature of high retrotransposon expression. The adjusted *p*-values obtained from differential expression analyses are shown.

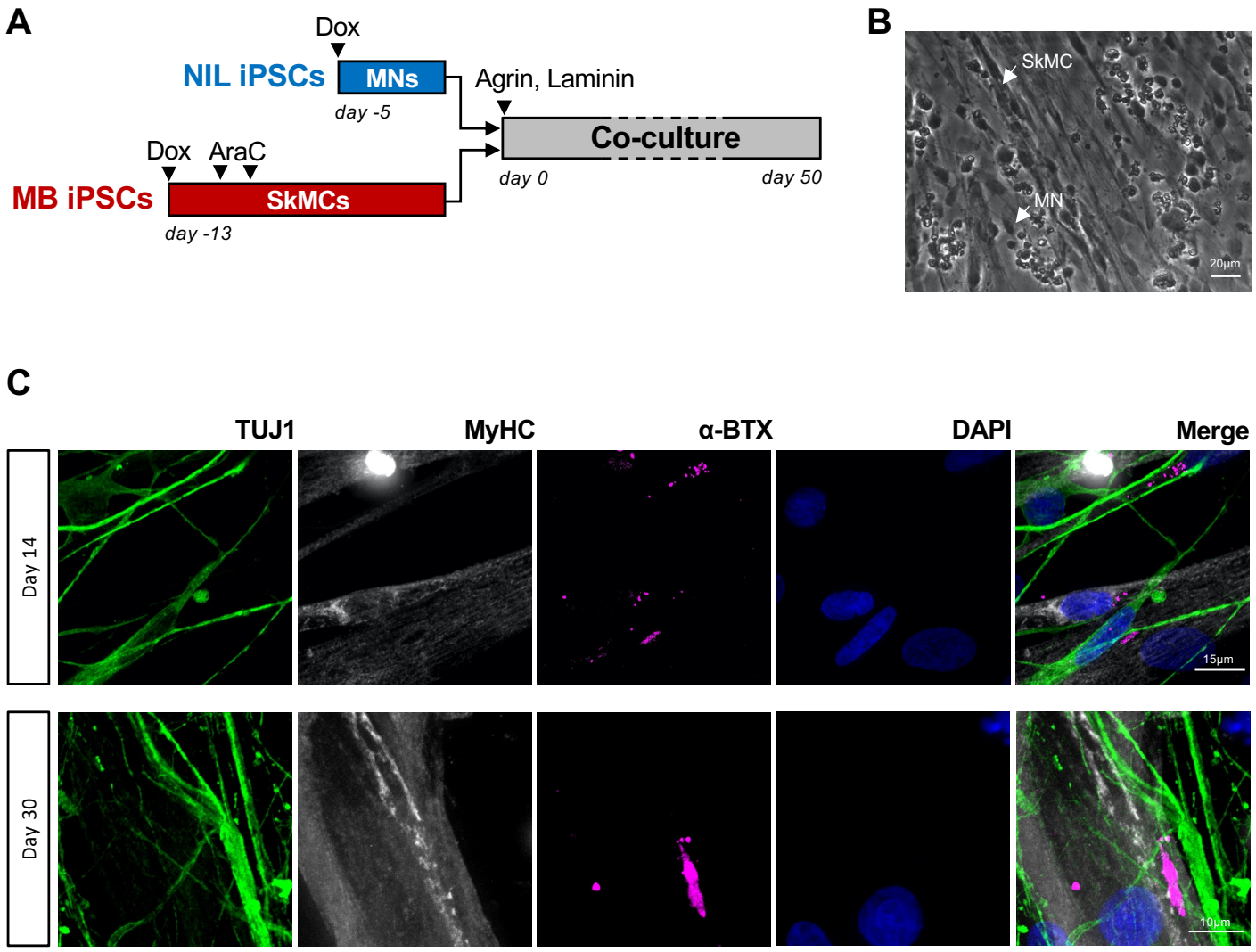
A
Dox
NIL iPSCs
MNs
day -5
Agrin, Laminin
Co-culture
day 0
day 50
Dox
AraC
MB iPSCs
SkMCs
day -13
B
SkMC
MN
20µm
C
TUJ1
MyHC
α-BTX
DAPI
Merge
Day 14
Day 30
15µm
10µm

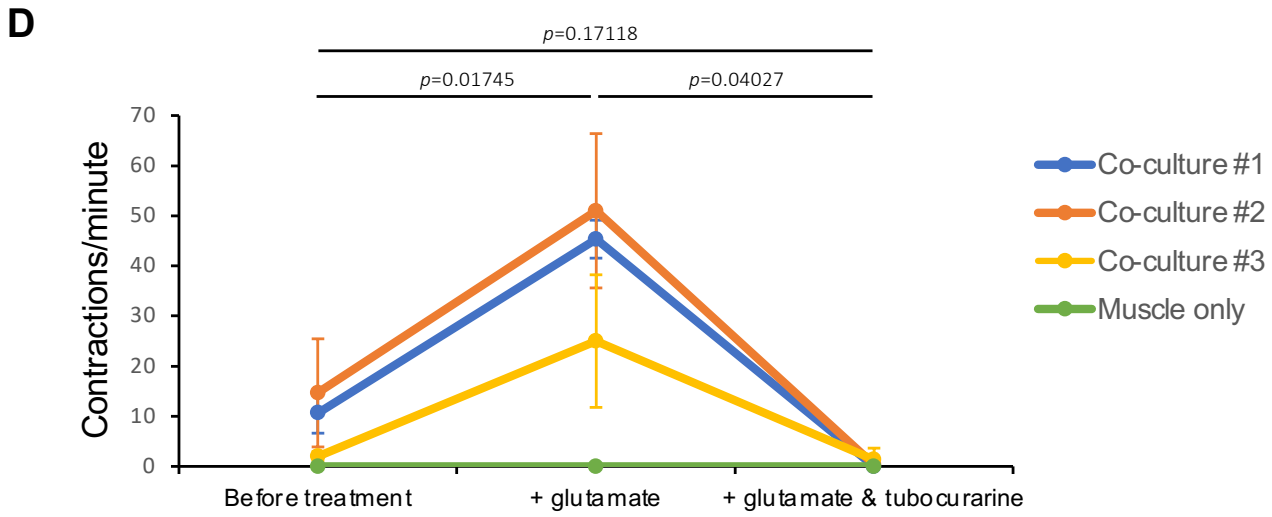
D
p=0.17118
p=0.01745
p=0.04027
Contractions/minute
70
60
50
40
30
20
10
0
Before treatment
+ glutamate
+ glutamate & tubocurarine
Co-culture #1
Co-culture #2
Co-culture #3
Muscle only

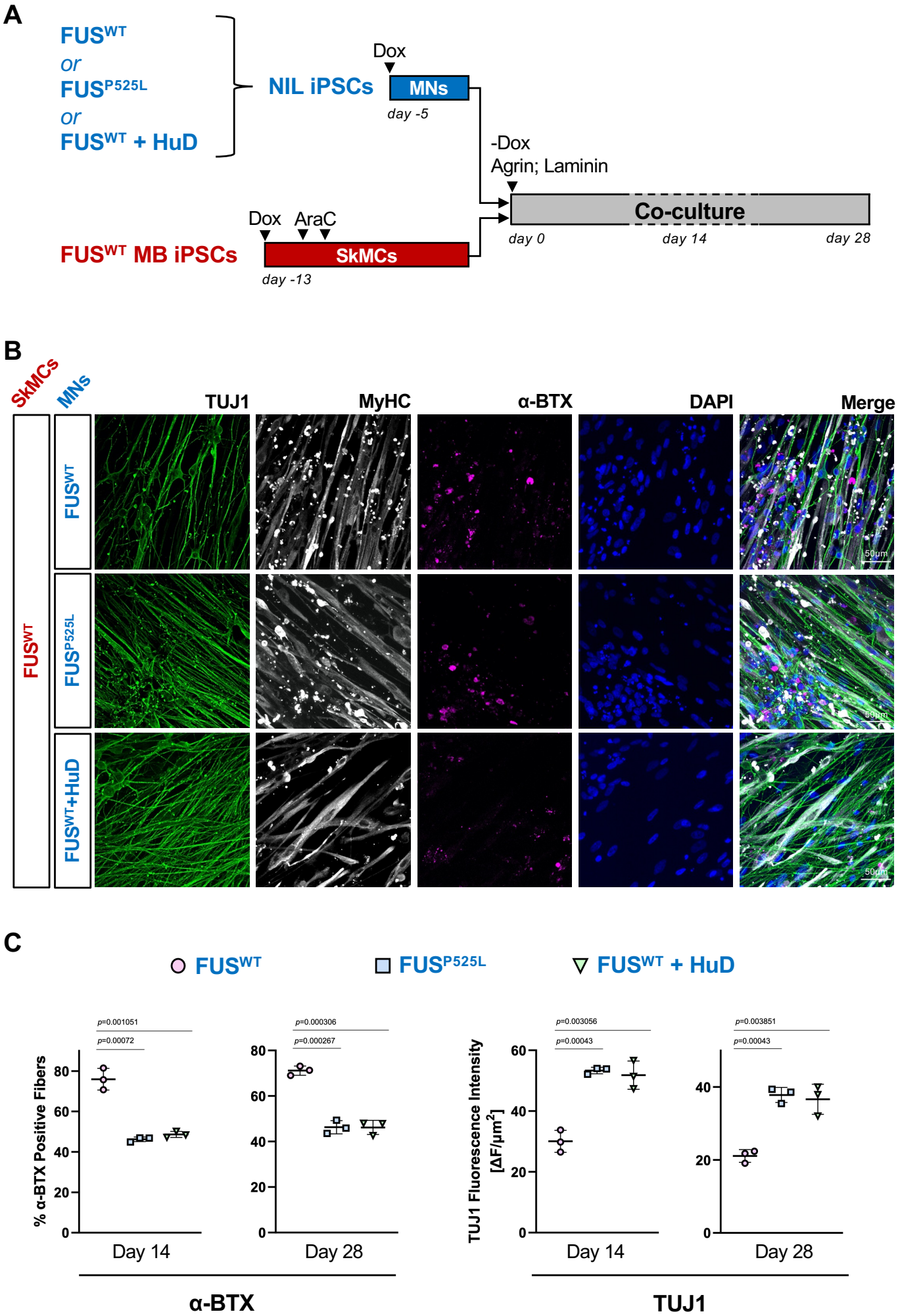
A
FUSWT
or
FUSP525L
or
FUSWT + HuD
NIL iPSCs
Dox
MNs
day -5
-Dox
Agrin; Laminin
Co-culture
day 0
day 14
day 28
Dox AraC
FUSWT MB iPSCs
SkMCs
day -13
B
SkMCs
MNs
TUJ1
MyHC
α-BTX
DAPI
Merge
FUSWT
FUSP525L
FUSWT+HuD
50µm
C
FUSWT
FUSP525L
FUSWT + HuD
% α-BTX Positive Fibers
p=0.001051
p=0.00072
p=0.000306
p=0.000267
Day 14
Day 28
α-BTX
TUJ1 Fluorescence Intensity [ΔF/µm2]
p=0.003056
p=0.00043
p=0.003851
p=0.00043
Day 14
Day 28
TUJ1

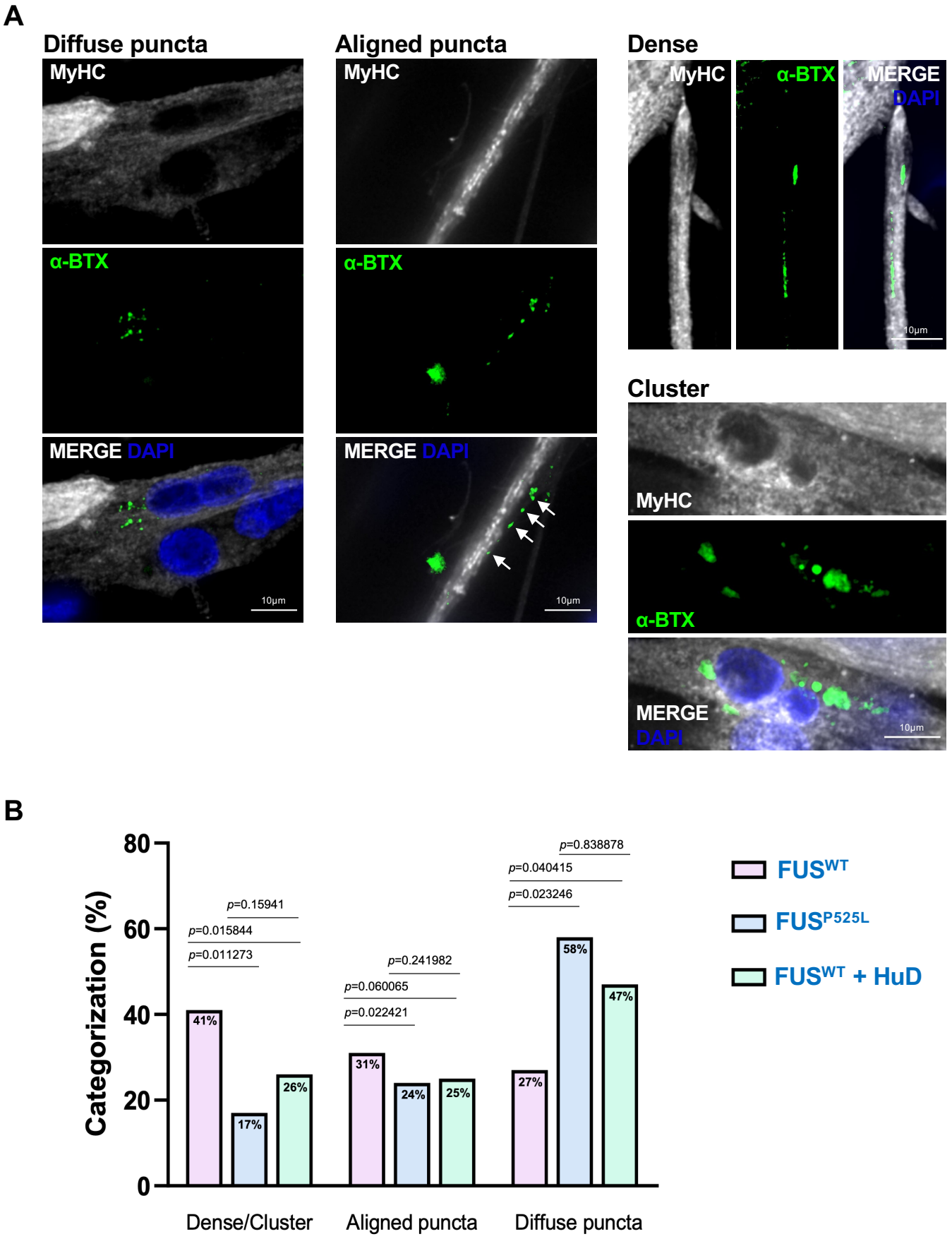
A
Diffuse puncta
MyHC
α-BTX
MERGE DAPI
10μm
Aligned puncta
MyHC
α-BTX
MERGE DAPI
10μm
Dense
MyHC
α-BTX
MERGE
DAPI
10μm
Cluster
MyHC
α-BTX
MERGE
DAPI
10μm
B
Categorization (%)
80
60
40
20
0
p=0.15941
p=0.015844
p=0.011273
41%
17%
26%
p=0.241982
p=0.060065
p=0.022421
31%
24%
25%
p=0.838878
p=0.040415
p=0.023246
27%
58%
47%
Dense/Cluster
Aligned puncta
Diffuse puncta
FUSWT
FUSP525L
FUSWT + HuD

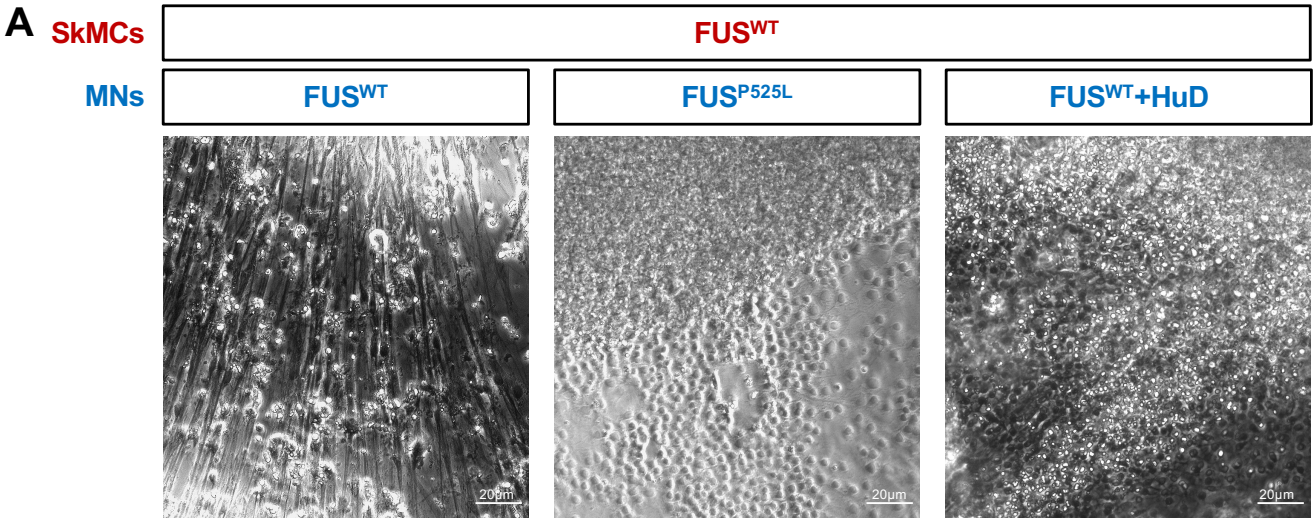
A
SkMCs
FUSWT
MNs
FUSWT
FUSP525L
FUSWT+HuD
20µm
20µm
20µm

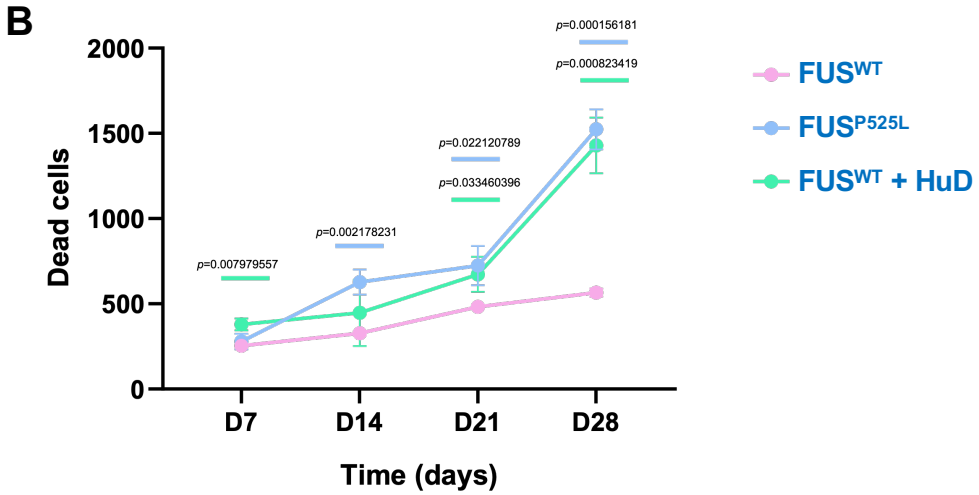
B
Dead cells
2000
1500
1000
500
0
D7
D14
D21
D28
Time (days)
p=0.007979557
p=0.002178231
p=0.022120789
p=0.033460396
p=0.000156181
p=0.000823419
FUSWT
FUSP525L
FUSWT + HuD

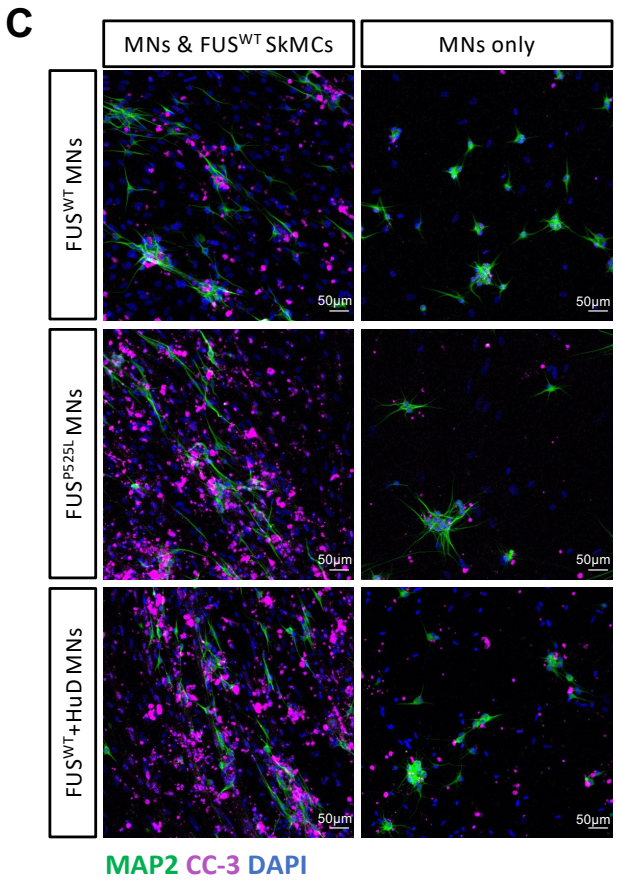
C
MNs & FUSWT SkMCs
MNs only
FUSWT MNs
FUSP525L MNs
FUSWT+HuD MNs
50µm
MAP2 CC-3 DAPI

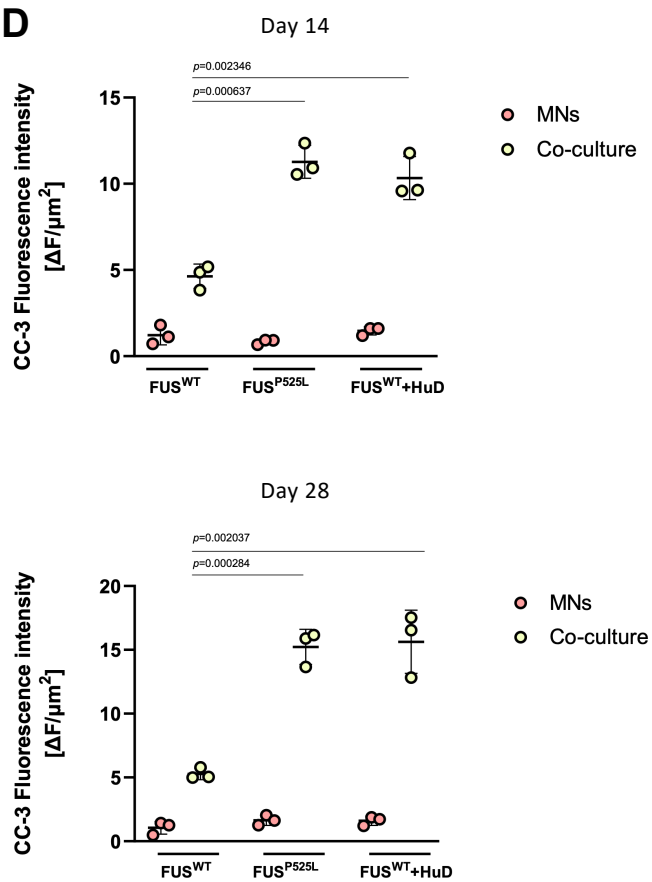
D
Day 14
CC-3 Fluorescence intensity [ΔF/µm2]
p=0.002346
p=0.000637
FUSWT
FUSP525L
FUSWT+HuD
MNs
Co-culture
Day 28
p=0.002037
p=0.000284

A

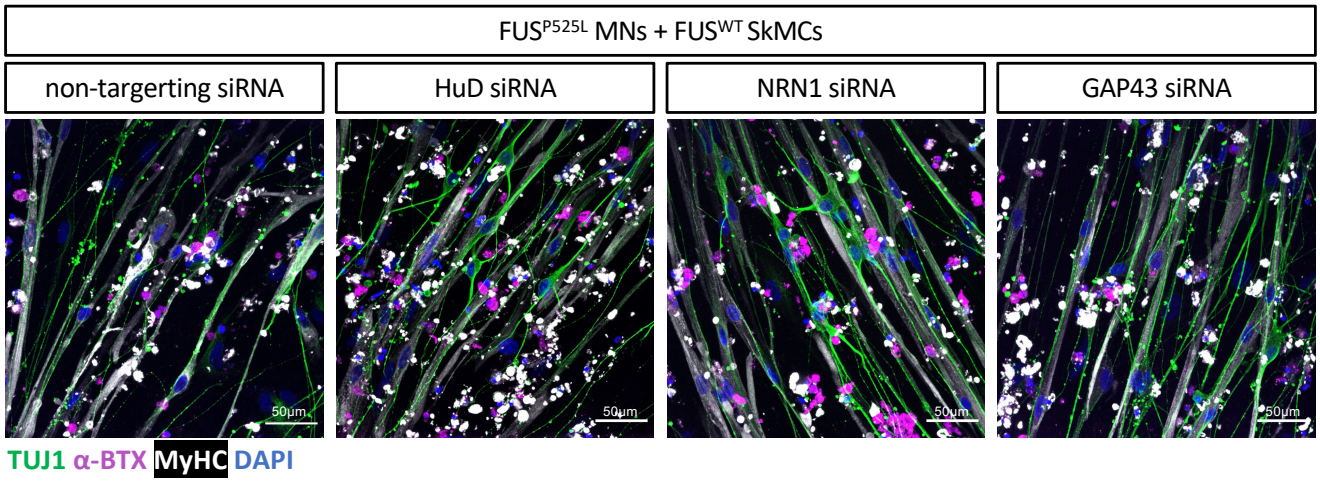
FUSP525L MNs + FUSWT SkMCs
non-targerting siRNA
HuD siRNA
NRN1 siRNA
GAP43 siRNA
50µm
TUJ1 α-BTX MyHC DAPI

B

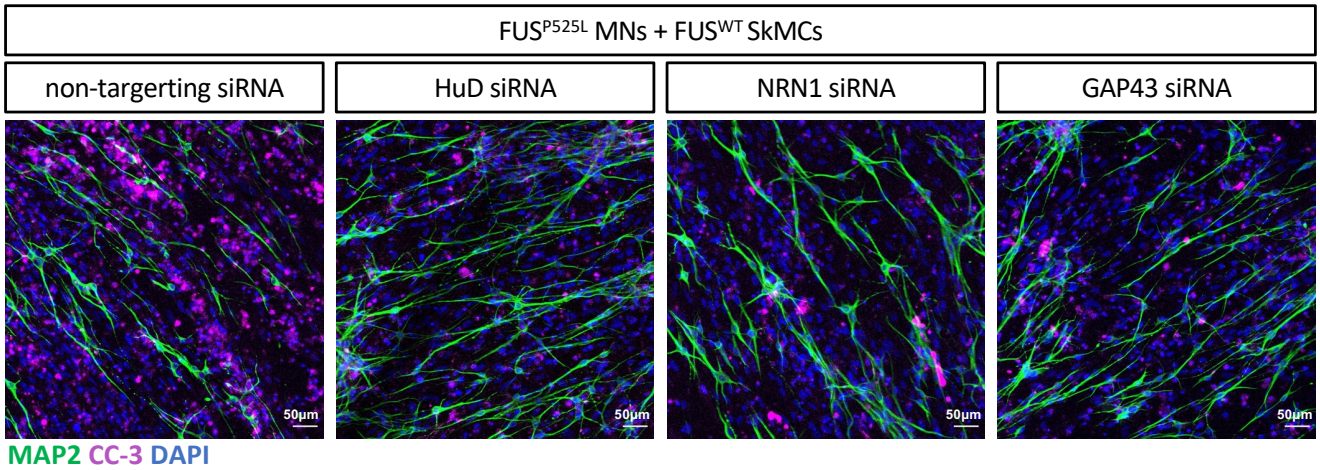
FUSP525L MNs + FUSWT SkMCs
non-targerting siRNA
HuD siRNA
NRN1 siRNA
GAP43 siRNA
50µm
MAP2 CC-3 DAPI

C

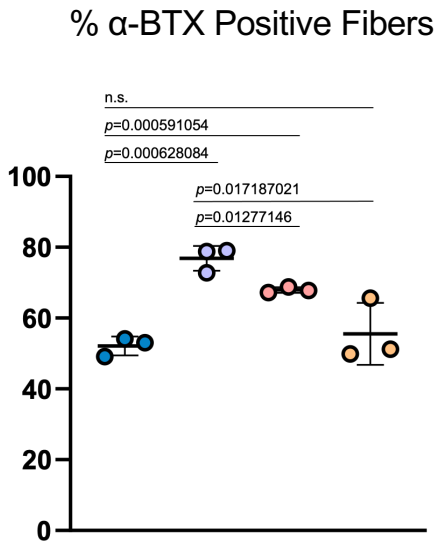
% α-BTX Positive Fibers
n.s.
p=0.000591054
p=0.000628084
p=0.017187021
p=0.01277146
100
80
60
40
20
0

D

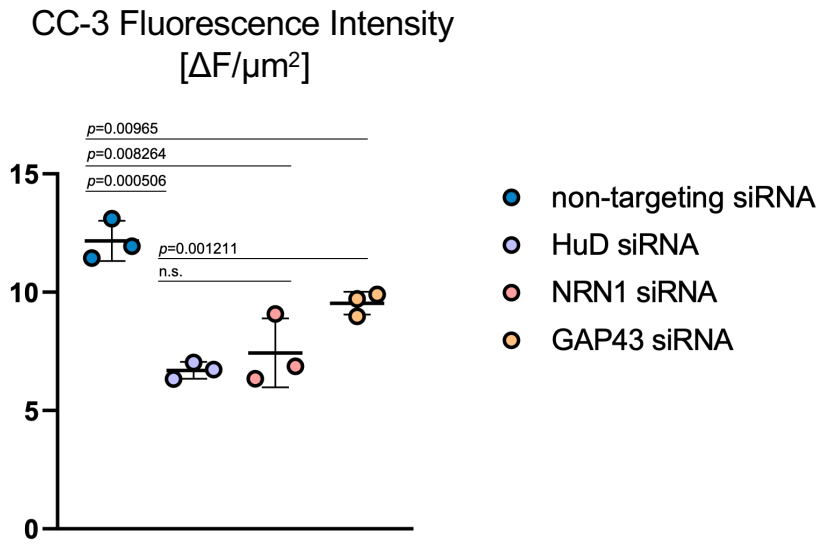
CC-3 Fluorescence Intensity
[ΔF/µm²]
p=0.00965
p=0.008264
p=0.000506
p=0.001211
n.s.
15
10
5
0
non-targeting siRNA
HuD siRNA
NRN1 siRNA
GAP43 siRNA

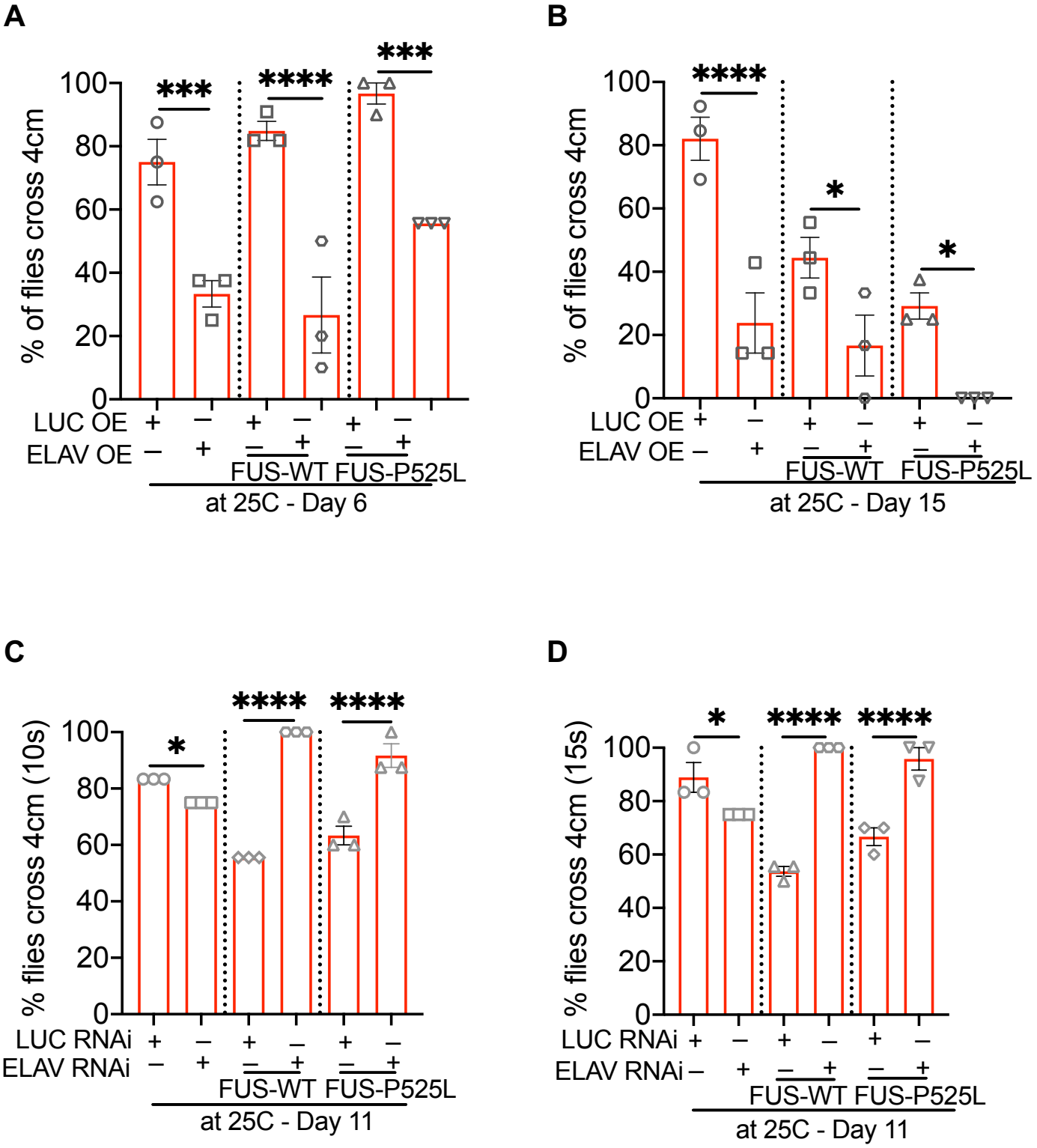
A
% of flies cross 4cm
100
80
60
40
20
0
***
****
***
LUC OE + – + – + –
ELAV OE – + – + – +
FUS-WT FUS-P525L
at 25C - Day 6
B
% of flies cross 4cm
****
*
*
LUC OE + – + – + –
ELAV OE – + – + – +
FUS-WT FUS-P525L
at 25C - Day 15
C
% flies cross 4cm (10s)
*
****
****
LUC RNAi + – + – + –
ELAV RNAi – + – + – +
FUS-WT FUS-P525L
at 25C - Day 11
D
% flies cross 4cm (15s)
*
****
****
LUC RNAi + – + – + –
ELAV RNAi – + – + – +
FUS-WT FUS-P525L
at 25C - Day 11

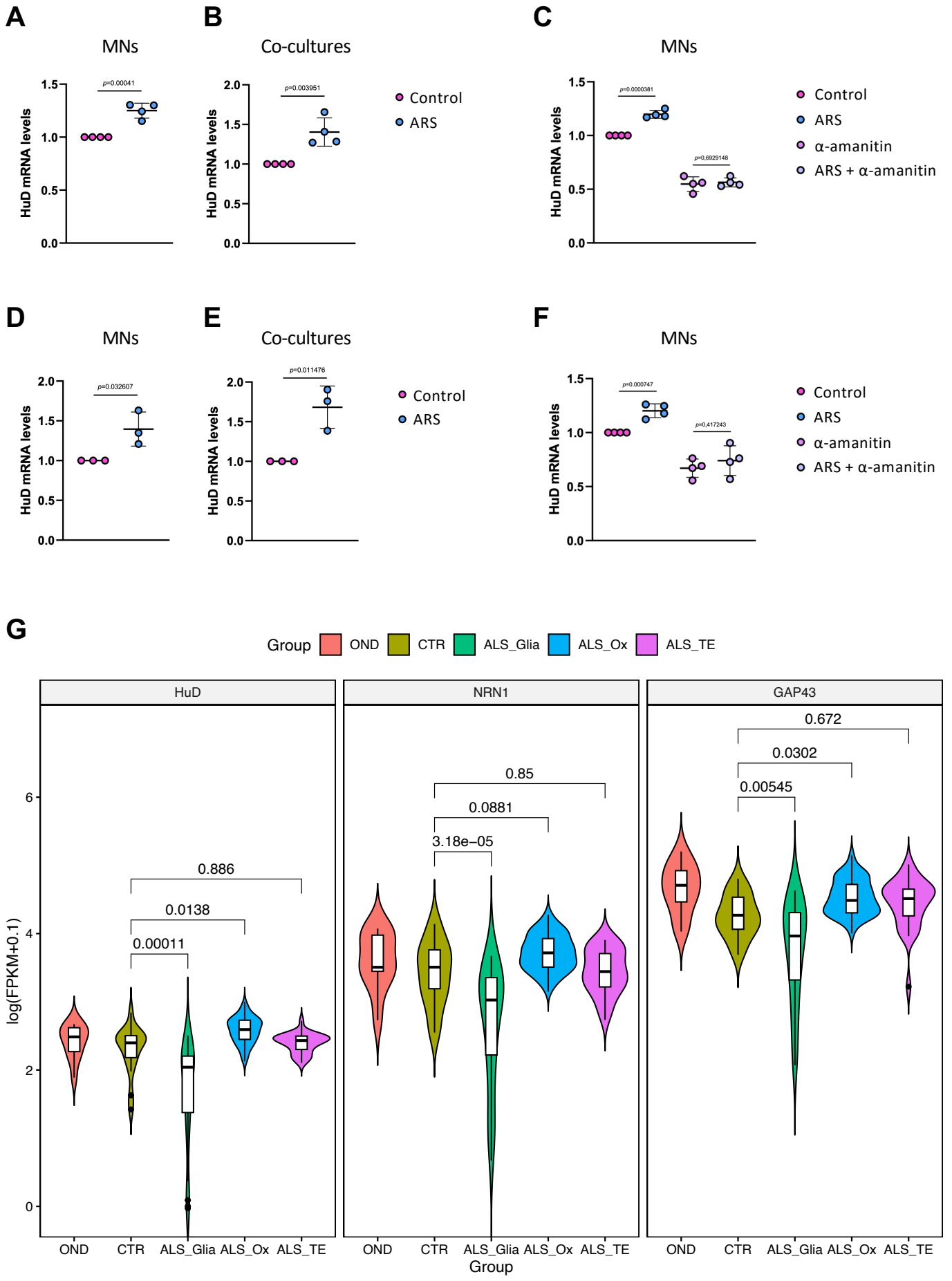
A
MNs
HuD mRNA levels
p=0.00041
B
Co-cultures
p=0.003951
Control
ARS
C
MNs
p=0.0000381
p=0,6929148
α-amanitin
ARS + α-amanitin
D
MNs
p=0.032607
E
Co-cultures
p=0.011476
F
MNs
p=0.000747
p=0,417243
G
Group
OND
CTR
ALS_Glia
ALS_Ox
ALS_TE
HuD
NRN1
GAP43
log(FPKM+0.1)
0.886
0.0138
0.00011
0.85
0.0881
3.18e−05
0.672
0.0302
0.00545